JOURNAL OF APPLIED PHYSICS VOLUME 83, NUMBER 7 1 APRIL 1998

X-ray diffraction studies of the effects of N incorporation in amorphous CN_x materials

J. K. Walters[a)]
Department of Physics and Astronomy, University College, Gower Street, London WC1E 6BT, United Kingdom

M. Kühn and C. Spaeth
Technical University Chemnitz-Zwickau, 09107 Chemnitz, Germany

E. Dooryhee
ESRF, B.P. 220, F-38043 Grenoble Cedex 9, France

R. J. Newport
Physics Laboratory, The University, Canterbury, Kent CT2 7NR, United Kingdom

(Received 21 October 1997; accepted for publication 22 December 1997)

The effects of nitrogen incorporation on the atomic-scale structure of amorphous CN_x samples have been studied for 0, 5, 20, and 30 at. % N concentration, by x-ray diffraction. Significant differences in the structure are observed on the incorporation of only 5 at. % N, and the changes in structure continue as further N is added. From the experimental data, we are able to obtain directly the average bond distances and then calculate the average bond angles for each of the samples. The average first neighbor distance shows a gradual decrease from 1.55 Å for 0 at. % N, to 1.44 Å for 30 at. % N, and a similar trend is observed in the position of the second neighbor peak. This gives a corresponding increase in the average bond angle from 108° to 114°. The results show an increase in the fraction of sp^2 bonded carbon atoms with increasing N concentration, and there is evidence for the presence of significant numbers of C≡N and C=N bonds. These results are also consistent with stress, hardness, and optical gap measurements for these samples. © *1998 American Institute of Physics.* [S0021-8979(98)03907-3]

I. INTRODUCTION

Carbon nitride materials have been a subject of considerable attention since the theoretical work of Liu and Cohen suggesting β-C_3N_4 as a hypothetical structure exhibiting attractive physical properties.[1] Further investigations with refined methods have shown that there are a variety of other crystalline structures, with different elemental compositions, which may have a similar structural stability.[2,3] However, only a few authors have reported the attempted experimental synthesis of crystalline carbon nitrides[4–6] and in the majority of the studies films with nitrogen contents significantly lower than 50 at. % and with a disordered structure have been found.[7–11] It is necessary to distinguish between hydrogen-free a-CN_x films and hydrogenated a-C:N:H, the latter being obtained when using a hydrocarbon precursor, as in most chemical vapor deposition (CVD) techniques.[12] Amorphous CN_x materials have interesting properties and a consequent range of potential applications—e.g., in the field of electronic materials, or wear protective coatings for magnetic storage devices.[13,14] In these cases, the nitrogen content in the films studied ranges from less than 1 at. % to about 30 at. %.

The investigation of the physical properties of CN_x has covered chemical composition, microstructure, electronic, optical, and mechanical properties but there is only limited knowledge of the atomic scale structure. In fact, direct information on the atomic arrangement is needed for reliable interpretation of data from analysis techniques, e.g., infrared (IR), x-ray photoelectron spectroscopy (XPS) or Raman spectroscopy.

X-ray diffraction experiments yield structural information averaged over the entire bulk sample, and provide the opportunity to obtain interatomic distances and bond angles directly. Thus far, diffraction studies of amorphous CN_x materials have been limited to electron diffraction,[15,16] although we have recently carried out complementary neutron diffraction measurements on two of the samples used in this study.[17]

We present the results of x-ray diffraction measurements on a series of four CN_x samples, with 0, 5, 20, and 30 at. % N, denoted ta-C, CN05, CN20, and CN30, and examine the effect of nitrogen incorporation on the atomic-scale structure of the material. The results are compared with those obtained from neutron diffraction measurements carried out on two of these samples,[17] and also with previously published electron diffraction data on a-C:N[15] and neutron diffraction on tetrahedral amorphous carbon (ta-C).[18] We also contrast this work with similar measurements previously carried out by two of the authors on the effects of N incorporation on a-C:N:H materials.[19] The effects of using an ion source to obtain high N content samples compared to deposition using nitrogen in the reactive plasma are discussed.

a)Electronic mail: j.walters@ucl.ac.uk

TABLE I. Preparation and compositional information on the four samples.

Sample	Deposition energy (eV)	N content (at. %)	Density (g cm^{-3})	Number density (atoms Å^{-3})	Stress, σ (GPa)	Hardness (GPa)	Optical gap (eV)
ta-C	C^+~20	0	2.8	0.14	5.4	56	1.8
CN05	C^+~20	5	2.7	0.13	4.0	45	0.75
CN20	C^+~20; N_2^+~100	20	2.2	0.11	2.7	37	...
CN30	C^+~20; N_2^+~200	30	2.0	0.10	1.7	9.5	0.22

II. EXPERIMENTAL DETAILS

A. Sample preparation

The samples were prepared by thin film deposition using a filtered cathodic arc. The arc discharge was operated with a cathode made from high purity graphite; the carbon plasma produced is highly ionized. A magnetic filter was used in order to separate macroparticles (of graphite) from the flux of film forming particles. Nitrogen could be incorporated into the growing film either by introducing a nitrogen gas flow into the deposition chamber, or by bombarding the substrate with a nitrogen ion beam from a Kaufman-type ion source—which proved necessary in order to obtain films with higher N contents, i.e., up to 30 at. %.[20] We have prepared four films, one without any nitrogen supply (ta-C), one with the nitrogen gas flow only (CN05), and two with the Kaufman ion source operated at 100 and 200 V beam voltage (CN20 and CN30, respectively). Gas flow rates of up to 8 sccm were used, yielding a total pressure in the range 0.01–0.02 Pa. For the nitrogen supply a special gas mixture with 10% of the ^{15}N-isotope was used to facilitate complementary nuclear magnetic resonance (NMR) studies on the same samples. The substrates were held at room temperature by means of a water-cooled substrate holder which was connected to ground potential. Ion current densities at the substrate have been measured prior to deposition for the cathodic arc plasma, j_C, and the Kaufman ion source, j_N, the measured values were $j_C \approx 1.5$ mA cm^{-2} (nearly constant in all experiments) and $j_N \approx 0.1/0.25$ mA cm^{-2} (for 100/200 V beam voltage).

Powder samples are required for the x-ray diffraction experiments: we therefore had to remove the film from the underlying substrate, and to collect the material from ten deposition runs. Applying a standard procedure from microelectronics technology, silicon wafers coated with photoresist were used as substrates; following film deposition the photoresist was dissolved in acetone and the CN_x material fell off the substrate as flaky powder. Repeated rinsing with high purity acetone was carried out to ensure no residual photoresist contamination. The material from several films prepared under identical conditions was collected and after vaporizing a small volume of remaining pure acetone, the CN_x powder was left. For each sample the amount of material obtained in this way was between 25 and 80 mg.

Information on the chemical composition and the mass density of the samples was inferred from elastic recoil detection analysis (ERDA) on films deposited onto silicon wafers under identical conditions. A summary of the characteristics of the four samples is given in Table I, and further data can be found in Ref. 20. Hardness measurements were performed using the nanoindentation method for films (thickness >1 μm) deposited on cemented carbide. ERDA yields hydrogen content values well below 1 at. %.

B. X-ray diffraction

The x-ray diffraction data presented here were obtained using standard flat-plate θ:2θ transmission diffraction geometry on station BM16[21] at the European Synchrotron Radiation Facility (ESRF), Grenoble, France. The high intensity beam provided by this synchrotron source is essential for making measurements on very small samples of relatively weak scattering materials. Data were collected for each sample and for the empty sample cell. The windows of the sample cell are made of Kapton, which has a well-known and relatively featureless diffraction pattern. The data were collected using x rays of wavelength 0.6 Å and were normalized to allow for variations in the incident flux. Corrections for detector deadtime, beam polarization, background scattering effects (including those from the sample container), absorption and the 2θ variation of the illuminated sample volume were made, with analysis based on the formalism described by Warren.[22]

For a system of N identical atoms the scattered intensity (in electron units) is given by

$$\frac{I(Q)}{N} = \sum_m f^2 + \sum_m f^2 \sum_{n \neq m} e^{iQr_{nm}}, \quad (1)$$

where f is the atomic form factor, r_{nm} is the distance between atoms n and m, and $Q = |\mathbf{Q}| = |\mathbf{k}_i - \mathbf{k}_f|$ is the wave vector transfer associated with the diffraction experiment—for elastic scattering $Q = (4\pi/\lambda)\sin\theta$, where 2$\theta$ is the scattering angle and λ is the x-ray wavelength. This equation represents both the intra-atomic (self-scattering) and interatomic (interference) scattering of the system. In the experimental data, a third component to the measured intensity is also collected which arises from the inelastic scattering of x rays by the sample. Some of the inelastic scattering is removed "at source" by the use of analyzer crystals placed in front of the detectors; however the small proportion that remains affects the data quite considerably, and a method of smooth curve fitting has to be applied. This involves fitting a low-order polynomial through the data to remove the underlying residual inelastic scattering curve until the data oscillates about the calculated self-scattering profile.

For systems of more than one atom type, an approximate method can be used to calculate the scattered x-ray intensity by choosing a convenient "unit of composition," u, for the material.

We can then define an average scattering factor per electron, f_e:

$$f_e=\frac{\Sigma_u f_m}{\Sigma_u Z_m}, \tag{2}$$

where the sum over u represents the weighted sum over the atoms of mass number Z_m. The form factor for each atom type can then be approximated by $f_m=K_m f_e$, where the effective electron numbers K_m will be approximately equal to Z_m.

For any given displacement $\mathbf{r}$, the electron density averaged over all directions is given by $\rho_j(\mathbf{r})$, where the subscript j represents the atom type. This shows fluctuations from the average electron density of the sample ρ_e. In an amorphous material there is no preferred orientation, so spherical symmetry can be assumed. Therefore, the sum over u can be replaced by an integral over the volume:

$$\frac{I_u(Q)}{N}-\sum_u f_j^2=f_e^2\sum_u K_j\int 4\pi r^2[\rho_j(r)-\rho_e]\frac{\sin Qr}{Qr}\,dr. \tag{3}$$

The left-hand side of the equation can be obtained from the experiment and is called the x-ray structure factor, $S(Q)$. In practice it is not trivial to measure the x-ray diffraction pattern in electron units, but an absolute intensity can be obtained by scaling the data to oscillate about the theoretical self-scattering term, which is subtracted to give $S(Q)$. The real-space total pair distribution function $G(r)=\rho(r)-\rho_e$ is a measure of the electronic density at a distance r from a given origin atom. $G(r)$ is obtained by direct Fourier transformation of the structure factor $S(Q)$. For this data, an $r_{\min}$ cut-off was also applied when taking the Fourier transform.[23] This is a variation on Fourier filtering in which a distance $r_{\min}$ is defined as the shortest bond length which is physically reasonable, and it therefore determines the start of the features in the $G(r)$. We can also obtain the radial distribution function, $J(r)$, where

$$J(r)=4\pi r^2\rho(r). \tag{4}$$

$J(r)$ is a measure of the number of atom centers at a given radial distance and can then be fitted with a series of Gaussians allowing position and area to vary. By this method accurate values for the bond lengths, and therefore also the bond angles can be determined. (In principle it is also possible to estimate absolute coordination numbers, but the difficulty in defining the Q-dependant form factors for a binary system renders this impossible in the absence of accurate corrections for Compton scattering, i.e., inelasticity effects.)

III. RESULTS AND DISCUSSION

Figure 1 shows the raw x-ray diffraction data collected for the four samples. Figures 2 and 3, respectively, show the total structure factors, $S(Q)$, and pair correlation functions, $G(r)$, obtained from the x-ray diffraction experiments for the samples described above.

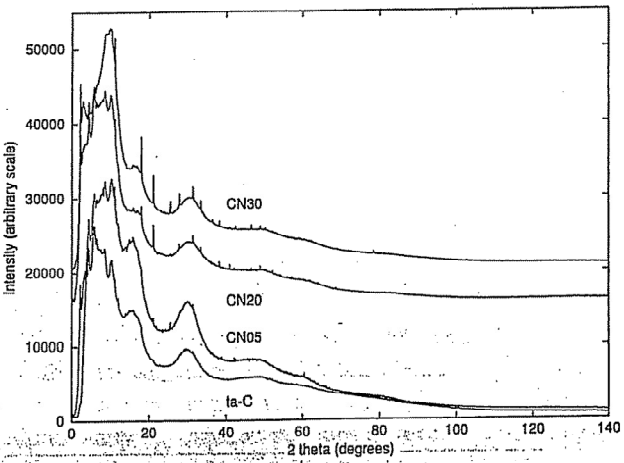

FIG. 1. Uncorrected x-ray diffraction data, showing the small Bragg peaks in the data for the four samples.

Considering the $S(Q)$ data in Fig. 2, it is clear that there are two pairs of similar spectra: samples ta-C and CN05, and then samples CN20 and CN30. At 0 and 5 at. % N there are six discernable peaks in the range of the experimental data. Small differences in the peak intensities can be seen between the data for ta-C and CN05: the very first small peak at $\sim$2.1 Å^{-1}, and the second peak at $\sim$3.4 Å^{-1} both increase in intensity going from 0 to 5 at. % N. There are also small differences beyond $\sim$4 Å^{-1}. Similarly, comparison of the data for CN20 and CN30 shows that the largest differences in the peak intensities occur at Q values below $\sim$4 Å^{-1}, and again the peaks show an increase in intensity with increasing N content. In the region 8–18 Å^{-1}, there are three peaks, which are all at slightly higher Q values in the higher N content samples CN20 and CN30. However, the changes in peak intensities are much smaller at high Q. The changes

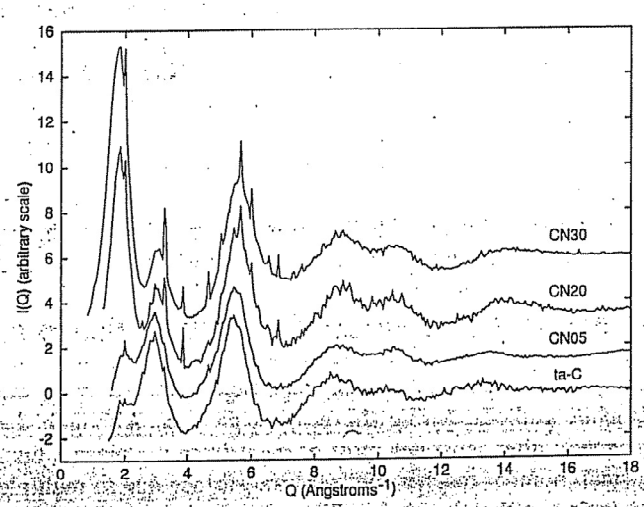

FIG. 2. The total structure factors, $S(Q)$, for the samples obtained after correction of the x-ray diffraction data.

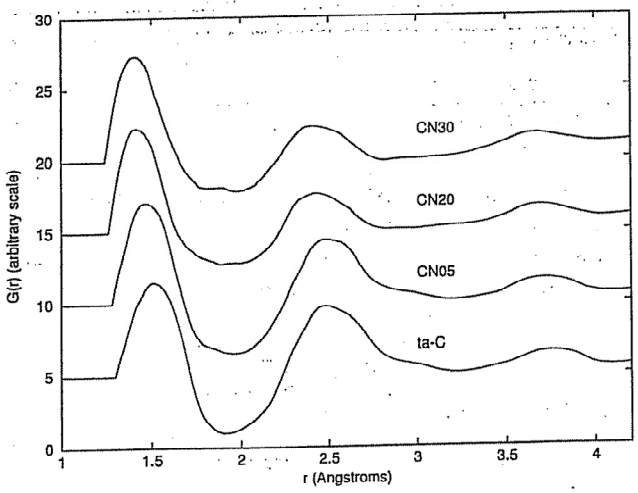

FIG. 3. The total pair correlation functions, $G(r)$, for the samples obtained by Fourier transformation of the total structure factors.

observed in these data match those seen in neutron diffraction data collected for samples CN05 and CN30.[17]

The biggest change by far is between samples CN05 and CN20 i.e., 5 and 20 at. % N. Throughout the range of the data sets there are differences in both peak intensities and peak positions. On increasing the N content from 5 to 20 at. %, the first peak ($\sim$2.1 Å^{-1}) shows a particularly large increase in intensity, together with a slight shift in position towards lower Q values. The second peak ($\sim$3.4 Å^{-1}) decreases in intensity, with the dip between these first two peaks becoming more pronounced. Also, there is a slight shift in the positions of both the dip and the second peak towards higher Q values. At $\sim$5.7 Å^{-1}, the change in peak intensity is smaller, but the peak position for CN20 is higher than for CN05. The width of this peak increases considerably in going from 5 to 20 at. % N. Similarly the dip ($\sim$7.0 Å^{-1}) following this peak is broadened at a higher Q value for CN20 than for CN05. Beyond $\sim$8 Å^{-1} the differences are smaller, but are still observable.

Notice from Figs. 1 and 2 (the uncorrected and corrected diffraction data) that there are small Bragg peaks present in each of the data sets, with more in the higher N content samples; these are most closely indexed using generic data for graphite. Similar features have been seen in x-ray diffraction data for a-C:N:H samples,[19] but they were not observed in neutron diffraction data due to the lower Q-space resolution. No Bragg peaks were seen in neutron diffraction data for samples CN05 and CN30.[17] It is important to note that in these new data, the Bragg peaks are small relative to the amorphous features in the data. This implies that while the samples may contain a few graphitic microcrystals, they do not have large crystalline inclusions. A possible source of this contamination is the macroparticles emitted from the graphite cathode during the erosion process. Although the magnetic filter separates most of them from the plasma flux, a small number reaches the substrate surface due to multiple bouncing at the chamber walls and is incorporated into the growing film. This problem was also seen in the ta-C samples of Gilkes *et al.*[18] deposited by the same method.

TABLE II. Results of the Gaussian fitting to the functions $J(r)$. (Data for the last two entries is from x-ray diffraction measurements on a-C:N:H samples taken from Ref. 19.)

Sample	N content (at. %)	1st neighbor peak position (±0.01 Å)	2nd neighbor peak position (±0.01 Å)	Average bond angle (±2°)
ta-C	0	1.55	2.51	108
CN05	5	1.50	2.50	113
CN20	20	1.45	2.43	114
CN30	30	1.44	2.42	114
a-C:N:H 1	0	1.43	2.51	123
a-C:N:H 4	10	1.39	2.46	124

However, this does not account for the increasing number and intensity of Bragg peaks in the higher N content samples CN20 and CN30. In order to obtain high N concentration in these samples, the growing film was bombarded by nitrogen ions using the Kaufman-type source. The energy of these ions, 100 and 200 eV, is such that it could cause graphitization in the small region around the ion impact site as the ion energy dissipates to the surrounding atoms, causing a relaxation of the structure. Again, this will not produce large graphitic inclusions, but could generate small, highly disordered, graphitic clusters with little or no interlayer alignment. This explanation is consistent with the observed increase of the intensity of the D band in Raman spectra for similar films.[20]

In summary, going from 0 to 5 at. % N and from 20 to 30 at. % N results in similar differences between the $S(Q)$ data sets. These differences are small, however, compared with the changes observed between 5 and 20 at. % N. We can therefore state that the addition of 5 at. % N to ta-C, and the addition of 10 at. % N to CN20 has only a small effect on the average, overall network structure, but that going from CN05 to CN20 induces a significant rearrangement in the structure. In order to understand what these differences mean in terms of specific structural changes, it is necessary to look at the Fourier transformed data, the total pair correlation functions $G(r)$.

The real-space data for the four samples is shown in Fig. 3. As with the reciprocal space data, there are clearly two pairs of similar data sets: samples ta-C and CN05 (low N content) and samples CN20 and CN30 (high N content). This is particularly obvious beyond $\sim$1.8 Å, and the data at lower r values reveal more subtle differences among all four samples. In the discussion of all the differences in the real-space data, it is necessary to consider the values given in Table II for the bond distances and angles determined by Gaussian fitting to the experimental $J(r)$ data.

Consider first the two low N concentration samples. The first neighbor peak moves from 1.55 Å for ta-C to 1.50 Å for CN05 and there is a corresponding movement of the second neighbor peak position from 2.51 to 2.50 Å. These changes result in an increase in the average bond angle from 108° to 113°. However, note that the peak positions used to evaluate the bond angle arises from a convolution of CC, CN, and NN correlations and, therefore, the average bond angle is not a

true CCC bond angle but results from an admixture of overlapping features. The data for ta-C here compares well with other diffraction data for tetrahedrally bonded amorphous carbon in the literature.[16,18] We can see that the incorporation of only 5 at. % N into the structure results in observable changes. Although the width of the first neighbor peak remains approximately constant, there is a decrease in the number of bonds at longer distances associated with sp^3 C–C single bonds, and an increase in the number of bonds at shorter distances. These changes have the overall effect of shifting the average bond length to a lower r value. The increased intensity at distances around 1.3–1.4 Å could be due to the formation of shorter bonds involving the smaller N atom and/or the conversion of sp^3 C–C single bonds to shorter olefinic or graphitic sp^2 C=C double bonds. The formation of CN, NN, or C=C bonds could all account for the observed differences in bond lengths and angles between these two samples. Similar changes were also seen in the samples studied by Davis *et al.*,[15] where they found a large increase in the fraction of sp^2 bonded C at ~5 at. % N.

For our samples, these trends continue as we move to the higher N content samples. From CN05 to CN20, the average first neighbor bond distance decreases further to 1.45 Å, which is closer to the value for crystalline graphite (1.42 Å).[24] The average bond angle for sample CN20 increases by a small amount to 114°. There is a further loss of intensity in the region associated with sp^3 C–C bonds, and an increase in the region of ~1.27 – 1.4 Å. Some of the increased intensity is associated with the formation of sp^2 C=C bonds, although not at distances below ~1.3 Å. At these short distances the intensity can only come from correlations involving the smaller N atoms, in the form of C≡N (~1.14 Å), C≈N (~1.30–1.36 Å), or C=N (~1.30 Å). Other possibilities are C≡C (~1.18 Å) and N=N (~1.24 Å) bonds. However, infrared spectroscopy data for amorphous CN_x samples shows features associated with C≡N and/or C=N bonds,[25–29] but C≡C and N=N bonds are not generally observed.[24,25,30] It would also be reasonable to assume the existence of C–N single bonds (~1.35–1.39 Å), although these cannot be resolved because of their similarity to sp^2 CC bond lengths.

Finally, for sample CN30 the position of the first and second neighbor peaks show a small decrease to 1.44 and 2.42 Å, respectively, giving the same average bond angle as for CN20, i.e., 114°. It is clear from these small differences, that the principle effects of incorporating a high N concentration have occurred by 20 at. % N. However, these data confirm that above 20 at. % N there are significant numbers of C=N and C≡N bonds in the network.

In addition to the differences between the bond distances and angles already discussed, there is evidence of a change in the nature of the second neighbor correlations between CN05 and CN20. In general, the peak at ~2.5 Å may safely be associated with CCC correlations, and is observed in many amorphous carbon materials.[18,19,31,32] In the two high N content samples studied here this peak is significantly less intense than for the two lower N content samples, whereas the same samples CN20 and CN30 show an increase in the intensity between the two peaks at ~1.9 Å. This phenomenon has also been observed in neutron diffraction data for CN05 and CN30,[17] and in electron diffraction data taken on similar amorphous CN samples.[15] It is most likely to be associated with the second-neighbor correlations arising from the increasing proportion of CCN groups, and/or site–site correlations associated with nanovoids arising from a reduced network connectivity but not actually involved in a pair of chemical bonds as such. A full discussion of this phenomenon was presented in our neutron diffraction paper.[17]

The changes we have observed between these samples, i.e.; the decrease in the average bond length and increase in the average bond angle, have confirmed the transition to a predominantly sp^2 bonded network as a result of incorporating N into the structure. This is accompanied by a number of changes in other properties of these materials (see Table I). For example, there is a decrease in the density, the stress, and the hardness of the samples with increasing N content, and a decrease in the optical band gap. All these measurements are consistent with a softer, more sp^2 bonded, network.

In our work on the effect of N doping on the structure of a-C:N:H[19] samples prepared using an ion beam deposition system from acetylene and nitrogen, the situation is complicated by the additional hydrogen, but similar changes were observed in increasing the N content from 0 to 10 at. %. The results from this study are summarized in Table II, along with those for these new amorphous CN_x samples. Although the network at 0 at. % N was already dominated by sp^2 CC bonds, a further significant decrease in the average first neighbor distance from 1.46 to 1.42 Å was observed, although the average bond angle remains unchanged within the experimental errors. In a-C:N:H only a very small increase in the number of C≡N and C=N bonds at ~1.2 Å was seen (probably due to the small amount of doping), although N–H bonds could be resolved. So, in these samples N plays a rather different role. The network already contains a large fraction of sp^2 bonded C. The added N converts only a small amount of sp^3 C to sp^2 C, and fits easily into the network causing little disruption to the average structure—only small differences are seen between a-C:H and the 10 at. % N doped sample.

In all our work on the effects of N incorporation on the structure of amorphous carbon materials, there is no doubt that the addition of N results in a relaxation of the network, creating a predominantly sp^2 bonded trigonal structure of carbon.

IV. CONCLUSIONS

The structure of a series of CN_x samples with 0, 5, 20, and 30 at. % N concentrations have been investigated using x-ray diffraction. The results obtained for ta-C (0 at. % N) are entirely consistent with those of other workers, namely that the material is predominantly a tetrahedrally bonded amorphous network. Some structural differences are evident with the introduction of only 5 at. % nitrogen: the average bond angle increases from 108° to 113°, indicative of both CN and/or NN bond formation and an increase in the number of sp^2 CC bonds. A more marked change occurs between 5

and 20 at. % (and 30 at. %) which, although qualitatively similar and following a consistent trend, reveals more clearly the growth of CCN mixed second neighbor correlations, some of which may be associated with correlations not directly involving chemical bonding. It is suggested that the composition dependence of a small, broadly graphitic, Bragg component to the data arises from the localized effects of the higher energy N ion implantation method used to achieve the higher nitrogen concentrations rather than being associated with contamination due to macroparticles. The trends in the data mirror those seen in the neutron diffraction data, and are also consistent the conclusions drawn from experimental measurements of hardness, stress, and optical gap.

To obtain more specific information about the local bonding environments, especially those involving N, other analysis techniques will be required, e.g., ^{15}N, ^{13}C, NMR, and IR spectroscopy, which are already underway. Also, comparison with models generated by computer simulations (using the methods of Ref. 33) may give further insight into atomic arrangements that are compatible with the diffraction data.

ACKNOWLEDGMENTS

J.K.W. acknowledges the generous support of the Royal 1851 Commission and the Royal Society. The project was also sponsored by the Bundesministerium für Bildung, Wissenschaft, Forschung and Technologie under Grant No. 03 N 5002 C. The authors are grateful to the ESRF for providing access to their x-ray research facilities, and to Th. Frauenheim for catalyzing this collaborative endeavor.

[1] A. Y. Liu and M. L. Cohen, Phys. Rev. B **41**, 10727 (1990).
[2] D. M. Teter and R. J. Hemley, Science **271**, 53 (1996).
[3] M. Coté and M. L. Cohen, Phys. Rev. B **55**, 5684 (1997).
[4] K. M. Yu, M. L. Cohen, E. E. Haller, W. L. Hansen, A. L. Liu, and I. C. Wu, Phys. Rev. B **49**, 5034 (1994).
[5] X. W. Su, H. W. Song, F. Z. Cui, and W. Z. Li, J. Phys. E **7**, 517 (1995).
[6] Y. Chen, L. Guo, and E. G. Wang, Philos. Mag. Lett. **75**, 155 (1997).
[7] C. A. Davis, D. R. McKenzie, Y. Yin, E. Kravtchinskaia, G. A. J. Amaratunga, and V. S. Veerasamy, Philos. Mag. B **69**, 1133 (1994).
[8] K. J. Boyd, D. Marton, S. S. Todorov, A. H. Al-Bayati, J. Kulik, R. A. Zuhr, and J. W. Rabalais, J. Vac. Sci. Technol. A **13**, 2110 (1995).
[9] D. Li, E. Cutiongco, Y.-W. Chung, M.-S. Wong, and W. D. Sproul, Diamond Films Technol. **5**, 261 (1995).
[10] Z. J. Zhang, J. Huang, S. Fan, and C. M. Lieber, Mater. Sci. Eng. A **209**, 5 (1996).
[11] H. Sjöström, L. Hultman, J.-E. Sundgren, and S. V. Hainsworth, J. Vac. Sci. Technol. A **14**, 56 (1996).
[12] F. L. Freire, G. Mariotto, C. A. Achete, and D. F. Franceschini, Surf. Coat. Technol. **74/75**, 382 (1995).
[13] J. Robertson and C. A. Davis, Diamond Relat. Mater. **4**, 441 (1995).
[14] E. C. Cutiongco, D. Li, Y.-W. Chung, and C. S. Bhatia, J. Tribology **118**, 543 (1996).
[15] C. A. Davis, Y. Yin, D. R. McKenzie, L. E. Hall, E. Kravtchinskaia, V. Keast, G. A. J. Amaratunga, and V. S. Veerasamy, J. Non-Cryst. Solids **170**, 46 (1994).
[16] A. R. Merchant, D. G. McCulloch, D. R. McKenzie, Y. Yin, L. E. Hall, and E. G. Gerstner, J. Appl. Phys. **79**, 6914 (1996).
[17] J. K. Walters, M. Kühn, C. Spaeth, H. Fischer, and R. J. Newport, Phys. Rev. B **56**, 14315 (1997).
[18] K. W. R. Gilkes, P. H. Gaskell, and J. Robertson, Phys. Rev. B **51**, 12303 (1995); K. W. R. Gilkes, P. H. Gaskell, and J. Yuan, J. Non-Cryst. Solids **164–166**, 1107 (1993).
[19] J. K. Walters, R. J. Newport, W. S. Howells, and G. Bushnell-Wye, J. Phys.: Condens. Matter **8**, 4739 (1996).
[20] C. Spaeth, M. Kühn, U. Kreissig, and F. Richter, Diamond Relat. Mater. **6**, 626 (1997).
[21] *ESRF Beamline Handbook*, edited by R. Mason (ESRF Internal Report, 4th Edition, January 1997); updated information on ESRF facilities is available at http://www.esrf.fr
[22] B. E. Warren, *X-ray Diffraction* (Dover, New York, 1990).
[23] A. K. Soper, in *Neutron Scattering Data Analysis 1990*, edited by M. W. Johnson, IOP conference Series (IOP, Bristol, 1990), Vol. 107, p. 57.
[24] *CRC Handbook of Chemistry and Physics. 75th Edition*, edited by D. R. Lide and H. P. R. Frederikse (CRC, Boca Raton, FL, 1994).
[25] T. Okada, S. Yamada, Y. Takeuchi, and T. Wada, J. Appl. Phys. **78**, 7416 (1995).
[26] J. H. Kaufman and S. Metin, Phys. Rev. B **39**, 13053 (1989).
[27] F. Rossi, B. Andre, A. van Veen, P. E. Mijnarends, H. Schut, F. Labohm, M. P. Delplancke, H. Dunlop, and E. Anger, Thin Solid Films **253**, 85 (1994).
[28] M. Friedrich, Th. Welzel, R. Rochotzki, H. Kupfer, and D. R. T. Zahn, Diamond Relat. Mater. **6**, 33 (1997).
[29] D. Lin, S. Lopez, Y. W. Chung, M. S. Wong, and W. D. Sproul, J. Vac. Sci. Technol. A **13**, 1063 (1995).
[30] H. Han and B. J. Feldman, Solid State Commun. **65**, 921 (1988).
[31] J. K. Walters, P. J. R. Honeybone, D. W. Huxley, R. J. Newport, and W. S. Howells, Phys. Rev. B **50**, 831 (1994).
[32] J. K. Walters, D. M. Fox, T. M. Burke, O. D. Weedon, R. J. Newport, and W. S. Howells, J. Chem. Phys. **101**, 4288 (1994).
[33] G. Jungnickel, M. Kühn, S. Deutschmann, F. Richter, U. Stephan, P. Blaudeck, and Th. Frauenheim, Diamond Relat. Mater. **3**, 1056 (1994).